This is the **submitted version** of the journal article:

Li, Jian; Slassi, Amine; Han, Xu; [et al.]. «Tuning the electronic bandgap of graphdiyne by H-substitution to promote interfacial charge carrier separation for enhanced photocatalytic hydrogen production». Advanced Functional Materials, Vol. 31, issue 29 (July 2021), art. 2100994. DOI 10.1002/adfm.202100994

This version is available at https://ddd.uab.cat/record/271952

Tuning the Electronic Bandgap of Graphdiyne by H-Substitution to Promote Interfacial Charge Carrier Separation for Enhanced Photocatalytic Hydrogen Production

By *Jian Li,[1] Amine Slassi,[2] Xu Han,[3] David Cornil,[2] Minh-Huong Ha-Thi,[4] Thomas Pino,[4] Damien P. Debecker,[5] Christophe Colbeau-justin,[1] Jordi Arbiol,[3,6] Jérôme Cornil,[2] Mohamed Nawfal Ghazzal[1]* *

[1] Université Paris-Saclay, UMR 8000 CNRS, Institut de Chimie Physique, 91405, Orsay, France.

[2] Laboratory for Chemistry of Novel Materials, University of Mons, Place du Parc 20, 7000 Mons, Belgium

[3] Catalan Institute of Nanoscience and Nanotechnology (ICN2), CSIC and BIST, Campus UAB, Bellaterra, 08193 Barcelona, Catalonia (Spain).

[4] Université Paris-Saclay, CNRS, Institut des Sciences Moléculaires d'Orsay, 91405, Orsay, France.

[5] Institute of Condensed Matter and Nanosciences (IMCN), UCLouvain, Place L. Pasteur 1, 1348 Louvain-la-Neuve, Belgium.

[6] ICREA, Pg. Lluís Companys 23, 08010 Barcelona, Catalonia (Spain).

*Correspondence and requests for materials should be addressed to Mohamed Nawfal Ghazzal (email: mohamed-nawfal.ghazzal@universite-paris-saclay.fr).

Abstract: Graphdiyne (GDY), which features a highly π-conjugated structure, direct bandgap and high charge carrier mobility, presents the major requirements for photocatalytic applications. Up to now, all photocatalytic studies were performed without paying too much attention on the GDY band gap (1.1 eV at the G_0W_0 many-body theory level). Such a narrow bandgap is not suitable for the band alignment between GDY and other semiconductors, making it difficult to achieve efficient photogenerated charge carrier separation. Herein, for the first time, we demonstrate that tuning the electronic bandgap of GDY via H-substitution (H-GDY) promotes interfacial charge separation and improves photocatalytic H_2 evolution. The H-GDY

exhibits an increased bandgap energy (~2.5 eV) and exploitable conduction band minimum and valance band maximum edges. As a representative semiconductor, TiO_2 was hybridized with both H-GDY and GDY to fabricate a heterojunction. Compared to the GDY/TiO_2 composite, the H-GDY/TiO_2 heterojunction leads to a remarkable enhancement of the photocatalytic H_2 generation by 1.35 times under UV-visible illumination (6200 μmol h^{-1} g^{-1}) and 4 times under visible light (670 μmol h^{-1} g^{-1}). Such enhancement is attributed to the suitable band alignment between H-GDY and TiO_2, which efficiently promotes the photogenerated electrons and hole separation, as supported by Density Functional Theory calculations.

1. Introduction

In a response to the urgent need for sustainable and clean energy source for the up-coming generations, photocatalytic hydrogen evolution involving light-irradiated semiconductors offers both a sustainable and relatively low-cost solution.[1-6] Along with the intensive research efforts in developing photocatalysts with high performance, low cost and environmental friendliness, carbon-based hybrid photocatalysts represented by graphene have emerged as a new alternative class of materials.[7-8] In order to maximize the charge carrier transport and separation, graphene-based hybrid photocatalysts require a preliminary opening of its zero bandgap, by either chemical modification or electric field control.[9-11] Compared to graphene, graphdiyne (GDY), a rapidly developing 2D carbon material, is an even more promising candidate for catalytic energy conversion, due to its inherent direct bandgap, high charge carrier mobility, and simple preparation methods.[12-20] Up to date, semiconductors including TiO_2, ZnO, CdS and C_3N_4, have been successfully hybridized with GDY for enhanced photocatalytic applications.[21-26] However, all these photocatalytic systems were developed without any optimization of the GDY bandgap. The narrow bandgap around 1.1 eV of pristine GDY neither meets the requirement to overcome the theoretical endothermic change in the process of water splitting (i.e., 1.23 eV),[27-28] nor achieve the interfacial separation of photogenerated charge

carriers to the maximum extent, because of the mismatch between the conduction/valence band edges of GDY and the donating/accepting energy levels of the other semiconductor. Tuning the bandgap of GDY in a hybrid system would provide a photosynthetic platform to mimic the "natural photosynthesis" for efficient hydrogen evolution. Type II heterostructured photocatalysts that possess adequate band alignment between two semiconductors are demonstrated to spatially separate the photogenerated charge carriers for highly efficient water reduction and oxidation to achieve water splitting.[29-30] Thus, tuning the electronic bandgap of GDY, to fabricate such a type II heterostructure represents a great potential for developing high-performance photocatalysts.

Chemical modification and element doping have been considered as effective approaches for adjusting the electronic band structure and related properties of carbon allotropes.[31-34] The traditional "top-down" doping method requires high temperature treatment under a specific atmosphere containing the heteroatom source, which is hard to control in term of doping sites (at either the acetylene moieties or the benzene rings) to achieve the targeted properties. Owing to the unique solution-synthesis method of GDY,[35-40] a controllable doping/substitution method using a monomer design strategy provides an ideal bottom-up solution for adjusting the electronic bandgap of GDY. Hydrogen-substituted graphdiyne (H-GDY), prepared by the coupling reaction of 1,3,5-triethynylbenzene monomer, appears to be a good candidate. On the one hand, the introduction of hydrogen atoms on the meta-positions of benzene rings maintains the large π-conjugated structure and excellent charge carrier mobility.[41] On the other hand, the introduction of H atoms has been demonstrated to enable enlarging the bandgap of carbon-based materials,[42-43] which is beneficial to target the construction of type II heterostructured photocatalysts.

Toward this end, H-GDY was prepared through the polymerization of 1,3,5-triethynylbenzene monomer using CuCl as a catalyst. Experiments and theoretical calculations indicated H-GDY possessed a bandgap energy of ~2.5 eV and exploitable conduction band minimum (CBM) and

valance band maximum (VBM) edges. As a proof of concept, TiO$_2$ was combined with H-GDY to fabricate a type II heterostructured photocatalyst. The H-GDY/TiO$_2$ heterojunction showed remarkable photocatalytic activity for H$_2$ generation, under both UV-visible and visible light excitation. DFT calculations attribute this enhancement to the strong interaction and the suitable band alignment between H-GDY and TiO$_2$, which promotes the interfacial separation of the photogenerated electrons and holes and the photosensitization of TiO$_2$ under visible light. TRMC measurements confirmed a longer charge carriers lifetime for H-GDY/TiO$_2$ (~0.33 μs), compared to GDY/TiO$_2$ (~0.24 μs), further evidencing an efficient interfacial charge separation between H-GDY and TiO$_2$. The concept of tuning the electronic band gap of GDY to promote interfacial charge separation opens a new avenue for GDY-based photocatalysts.

2. Results and Discussion

We have first characterized the electronic structure of an isolated sheet of H-GDY versus GDY at the Density Functional Theory (DFT) level using periodic boundary conditions and the Perdew−Burke−Ernzerhof (PBE) functional within the Generalized Gradient Approximation (GGA) in order to describe on a relative basis the changes in the electronic structure when going from GDY to H-GDY. Figure 1 displays the band structure and the corresponding Density of States (DOS) together with the shape of the HOMO and LUMO orbital of the unit cell. The bandgap of GDY is calculated to be 0.46 eV and the width of the valence band to be 1.81 eV, in good agreement with previous calculations.[27-28] As expected, the bandgap calculated at the PBE level is lower than the quasi-particle bandgap of 1.1 eV found at the GW many-body theory level due to the well-established underestimation of electronic bandgaps with GGA functionals. Nevertheless, comparing at the GGA level the relative values of the bandgap of two different materials and the relative alignment of their valence or conduction band edges is meaningful, which thus will not affect the interpretation of the experimental results based on our calculations. The theoretical results reveal that the hydrogenation of graphdiyne (H-GDY) induces the opening of the band gap up to 2.40 eV, while the width of valence band is reduced to 0.82 eV.

Those trends are rationalized by the fact that all benzene rings are connected in meta positions in H-GDY, thus limiting the degree of conjugation and hence increasing the gap. Such change is also expected to impact the electronic coupling between the unit cells and hence the mobility of the charge carriers, as evidenced by the flattening of the CB and VB edges in Figure 1b. The positions of the VB and CB edges of GDY (H-GDY) are calculated to be -4.92 and -5.37 eV (-3.50 and -5.83 eV), respectively, which translates into a downward shift by 1.42 eV of the VB edge and an upward shift by 0.46 eV of the CB edge when going from GDY to H-GDY.
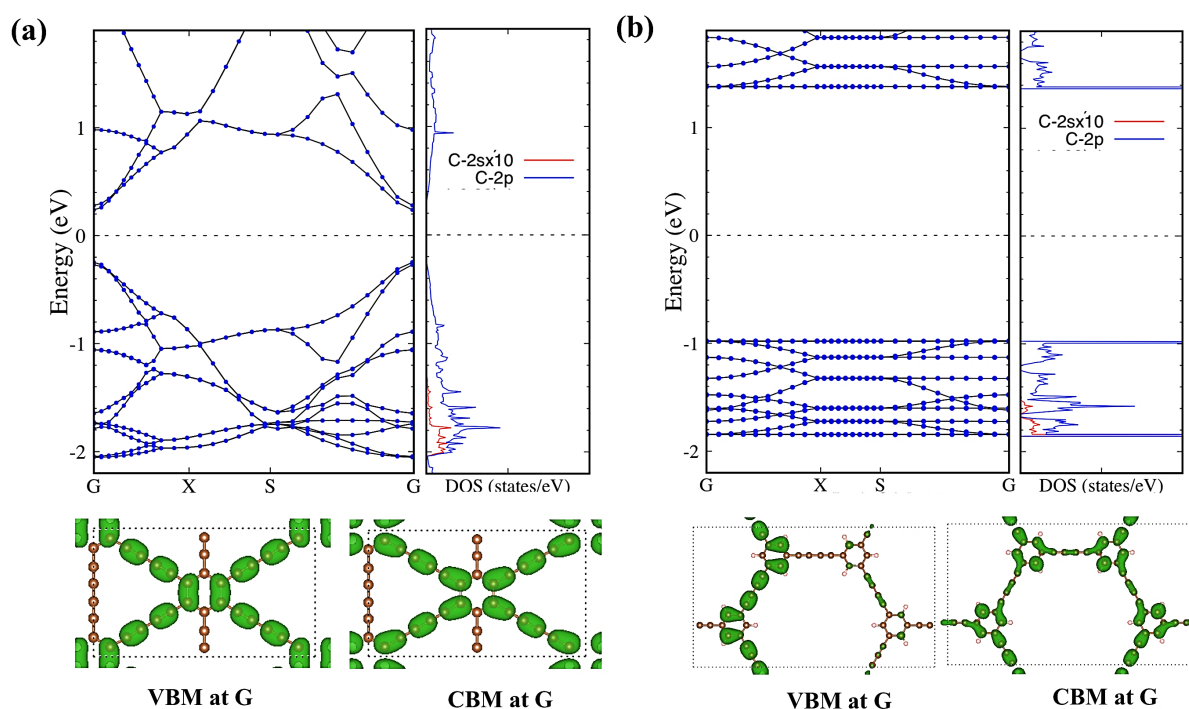
Figure 1. Band structure and projected density of states on the carbon orbitals of GDY (a) and H-GDY (b) calculated at the DFT level and shape of the HOMO and LUMO levels of the unit cell.

H-GDY was then synthesized via the coupling reaction of 1,3,5-triethynylbenzene monomer. In brief, 1,3,5-triethynylbenzene and CuCl were firstly added in pyridine and then heated at 60 °C for 24 h (Figure 2a). The presence of oxygen stimulated the formation of Cu I/II species, which catalysed the coupling reactions of the monomer to yield a yellowish powder (H-GDY). Raman spectroscopy, a useful technique for carbon materials, was used to study the bonding structure of the prepared H-GDY. Compared to the terminal C≡C stretching mode at 2123 cm^{-1}

in the monomer (Figure S1), the shifted peak at 2224 cm^{-1} in H-GDY confirmed the successful formation of conjugated diacetylenic linkages (Figure. 2b). The peaks located at 997 and 1589 cm^{-1} are attributed to the ring breathing and ring stretching of aromatic moieties, respectively.[44] Transmission electron microscopy (TEM) displayed that the prepared H-GDY was composed of dispersed thin layers, which promote the adsorption of solvent and fast charge transfer (Figure S2). X-ray photoelectron spectroscopy (XPS) revealed that the prepared H-GDY powder mainly contained elemental carbon and oxygen while no Cu species were detected, indicating that they were successfully removed (Figure 2c). Deconvolution of the high-resolution C 1s spectra displayed the major fractions of sp and sp^2 hybridized carbons with binding energies at 284.5 and 285.1 eV, respectively (Figure 2d). The additional oxygen atoms could originate from the partial oxidation of terminal alkyne units. In comparison to the monomer, an obvious bathochromic shift was observed in the UV−visible spectrum (Figure 2e), suggesting enlarged electron delocalization by the extended conjugated π-system. The optical bandgap (E_g) estimated from the Tauc plot is 2.50 eV (Figure 2f), which is in agreement with the DFT calculations. Such a bandgap is large enough to overcome the theoretical endothermic change associated to the process of water splitting (i.e., 1.23 eV). The valence band edge of H-GDY was determined by high resolution XPS to be 1.24 V vs NHE (Figure 2g). Combined to the bandgap of 2.50 eV, the conduction band and valence band edges of H-GDY are calculated at -1.26 V and 1.24 V vs NHE (-3.24 eV and -5.74 eV vs vacuum level), respectively. The DFT calculations and the experimental determination of the bandgap, CB and VB energy levels are in good agreement.
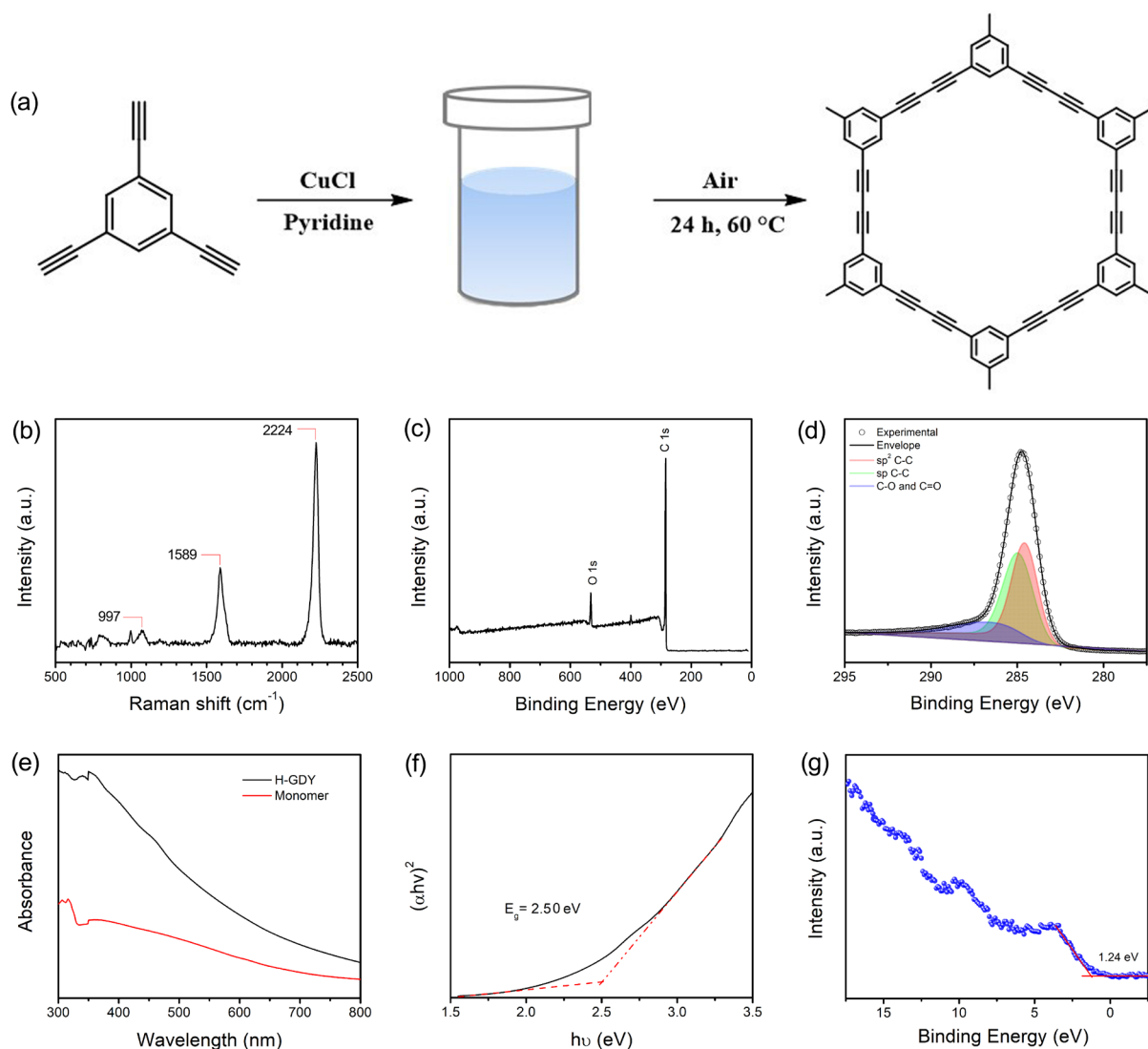
Figure 2. The synthesis and characterization of H-GDY. (a) Schematic illustration of the synthesis of H-GDY powder; (b) Raman spectrum of H-GDY; (c) XPS survey spectrum and (d) high-resolution C 1s spectrum of H-GDY; (e) UV-vis absorption spectrum and (f) Tauc plot of H-GDY; (g) high-resolution XPS valence band spectrum of H-GDY.

In order to demonstrate the potential of tuning the bandgap of GDY by H-substitution to fabricate type II heterojunction, TiO_2 was chosen as a model semiconductor to be interfaced with H-GDY. The microstructure of $H-GDY/TiO_2$ composite was firstly characterized by transmission electron microscopy (TEM) and the results were shown in Figures 3a and 3b. The images indicated that the TiO_2 nanoparticles were dispersed with particle size of about 20 nm (Figure 3a). The high resolution TEM (HRTEM) micrograph taken from one of them in Figure 3b revealed that this nanoparticle had a crystal phase in agreement with TiO_2 Anatase (space

7

group = I41/AMDS) with a=3.7850 Å b=3.7850 Å and c= 9.5140 Å (Figure 3b). The electron energy loss spectroscopy (EELS) compositional mapping of the selected region displayed a homogeneous distribution of both Ti and O. The spatial distribution of C was different from that of Ti and O elements, indicating that the sample had two composite phases (Figure 3c). X-ray diffraction (XRD), Raman spectra, and XPS were performed to investigate the composition and chemical state of H-GDY/TiO$_2$ composite. The XRD of TiO$_2$ exhibited a mixture of anatase and rutile crystalline phase, typical of P25, with the anatase (101) preferential orientation. No typical diffraction patterns for H-GDY were observed, probably due to their relatively low amount and crystallinity (Figure 3d). Compared to pristine TiO$_2$, the H-GDY/TiO$_2$ composites exhibit enhanced characteristic peaks of H-GDY at 1587 cm^{-1} and 2223 cm^{-1} with the increase of H-GDY content, confirming the successful blending (Figure 3e). The high-resolution Ti 2p peak for H-GDY/TiO$_2$ was resolved at the same binding energy, indicating that the valence band states of Ti have not changed upon coupling (Figure S3). UV-visible diffuse reflectance spectra demonstrated that the introduction of H-GDY redshifted the absorption of TiO$_2$ (Figure S4). The hybridization of GDY and TiO$_2$ was also characterized and the Raman spectra and TEM images of 5% GDY/TiO$_2$ were presented in Figure S5 and S6.
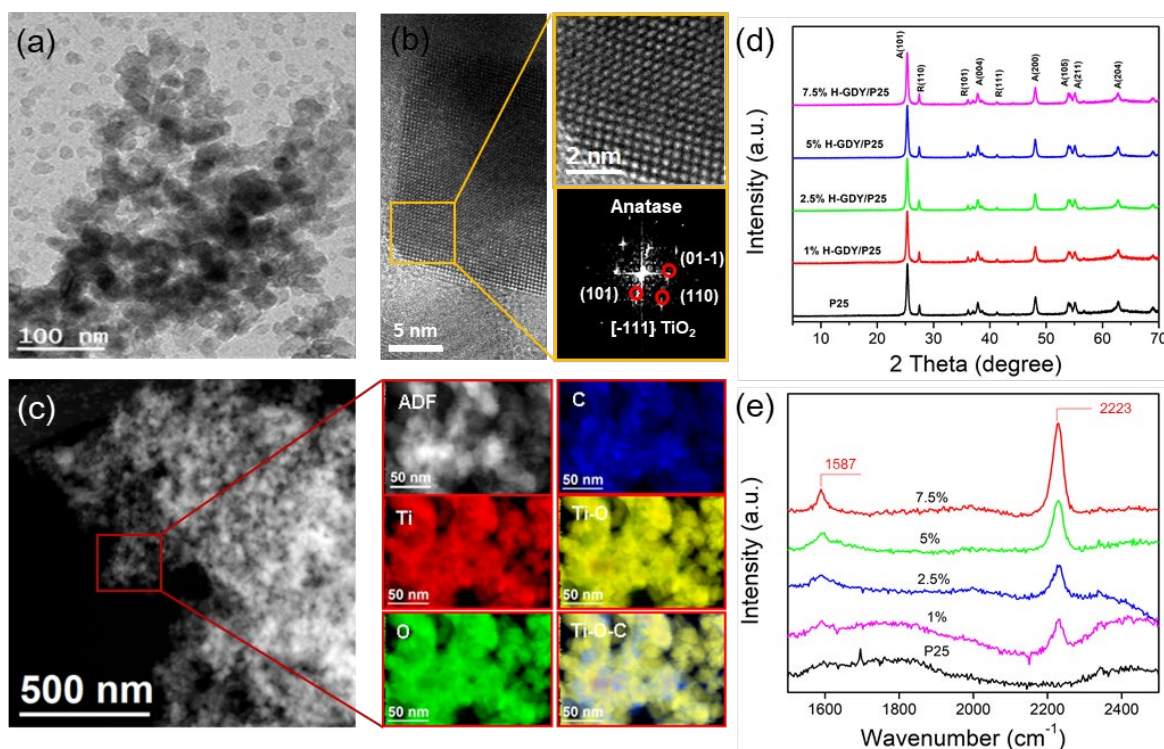
Figure 3. Characterization of H-GDY/TiO$_2$; (a) TEM image of H-GDY/TiO$_2$; (b) HRTEM micrograph, detail of the orange squared region and its corresponding power spectrum; (c) EELS mapping of selected region in H-GDY/TiO$_2$; (d) XRD patterns and (e) Raman spectra of TiO$_2$ and H-GDY/TiO$_2$ with different content of H-GDY.

The photocatalytic activity of the H-GDY/TiO$_2$ nanocomposite was evaluated towards H$_2$ generation in methanol/water solution (1:3 v/v) under Xenon lamp illumination. The photocatalytic activity of pristine TiO$_2$, which showed negligible H$_2$ generation, was improved remarkably when mixed with H-GDY. The photocatalytic activity increased with the content of H-GDY and reached an optimal efficiency for 5% H-GDY/TiO$_2$ (Figure 4a). The total amount of H$_2$ generated is up to 370 μmol after 6 hours, corresponding to ~6200 μmol h^{-1} g^{-1} H$_2$ production rate (Figure 4b). A further increase in the H-GDY content reduces the photocatalytic performance. This result suggests that a higher coverage of the TiO$_2$ surface reduces the accessibility to the active sites on the TiO$_2$ surface. In order to assess the stability of the photocatalysts, the optimal 5% H-GDY/TiO$_2$ sample was subjected to four consecutive test cycles of hydrogen evolution (Figure 4c). The 5% H-GDY/TiO$_2$ sustained a stable photoactivity for hydrogen evolution after four cycles under identical experimental conditions.

For comparison, GDY was synthesized and hybridized with TiO_2 under the same conditions. Both H-GDY/TiO_2 and GDY/TiO_2 composites displayed much higher photocatalytic efficiencies than those of pure TiO_2 (Figure 4d, 4e), which is attributed to the synergetic charge transfer processes in the composites. Notably, the H_2 generated rate of the 5% H-GDY/TiO_2 were 1.35 times and 4 times higher than those of the 5% GDY/TiO_2 under UV-visible and visible light, respectively. Such results point to the more efficient interfacial separation of photogenerated carriers between H-GDY and TiO_2. Excitingly, the H-GDY/TiO_2 even generate nearly 11 µmol H_2 from pure water after 8 h illumination, nearly 1.6 times that of GDY/TiO_2 (Figure 4f), further indicating the great potential of bandgap engineering of GDY for enhancing the photocatalytic efficiency.
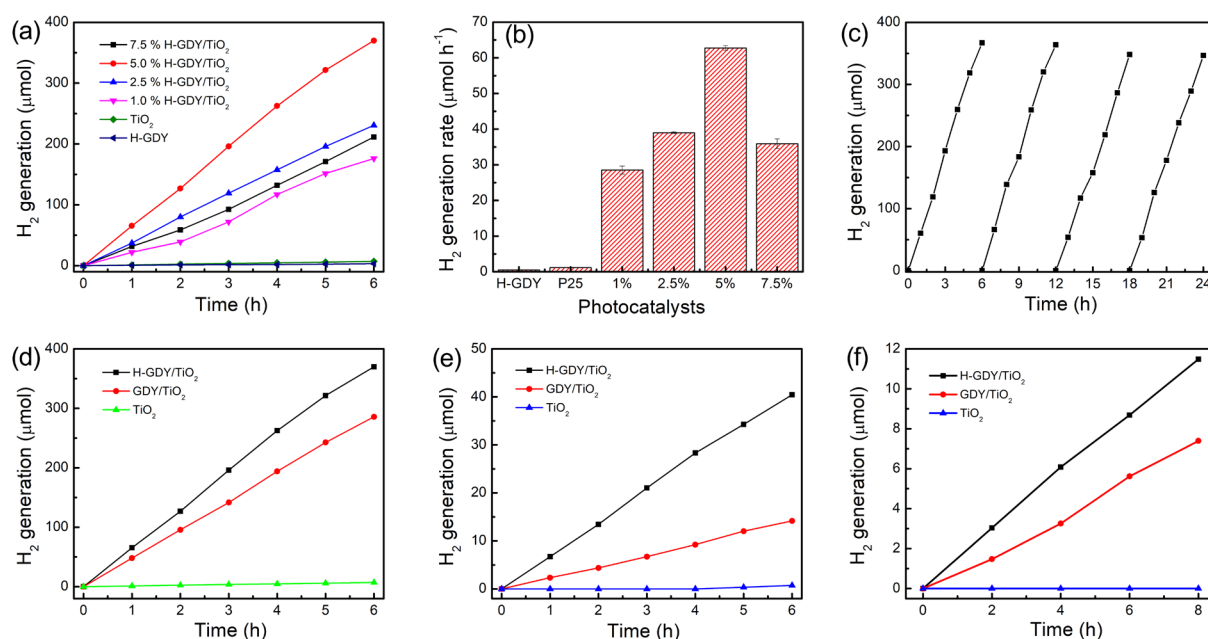
**Figure 4.** Photocatalytic characterization of different samples. (a) Photocatalytic activity and (b) H_2 generation rate for H-GDY/TiO_2 composites with different contents; (c) stability test of 5% H-GDY/TiO_2 photocatalyst; (d) photocatalytic activity of H-GDY/TiO_2, GDY/TiO_2 and TiO_2 composites under Xenon lamp; (e) photocatalytic activity of H-GDY/TiO_2, GDY/TiO_2 and TiO_2 composites under Xenon lamp illumination with 405 filter; (f) photocatalytic activity of H-GDY/TiO_2, GDY/TiO_2 and TiO_2 composites in pure water under Xenon lamp illumination.

DFT calculations were performed to shine light on the effect of H-substitution of the GDY on the properties of the hybrid systems made with TiO$_2$. For the sake of comparison with our experimental observations, we considered electron transfer processes only over the main exposed surface (101) of TiO$_2$, which is non polar. The optimized structures of the built TiO$_2$/GDY (H-GDY) interfaces are given in Figure S7 and the projected band structure of the hybrid system in Figure S8. We have calculated at DFT/PBE level with van der Waals corrections the interaction energy between the two components by the following equation:

$$E_{int} = E_{tot} - E_{TiO_2} - E_{(GDY/H-GDY)} \qquad (1)$$

Where E_{tot}, E_{TiO_2} and $E_{(GDY/H-GDY)}$ are the total energies of the heterostructure, individual TiO$_2$ and individual GDY (H-GDY) layers, respectively, in the geometry of the fully relaxed heterostructure.

The GDY (H-GDY) monolayer and the top layer of the TiO$_2$ surface undergo only a negligible buckling at the interfaces. The distance between H-GDY and TiO$_2$ (2.57 Å) is smaller than that computed between GDY and TiO$_2$ (2.75 Å). The calculated binding energies are found to be systematically twice larger in TiO$_2$/GDY compared to TiO$_2$/H-GDY heterostructures (-7.32 eV versus -4.20 eV, respectively). This points to the stronger interactions between H-GDY and TiO$_2$, which is expected to be beneficial for the interfacial charge transfer.
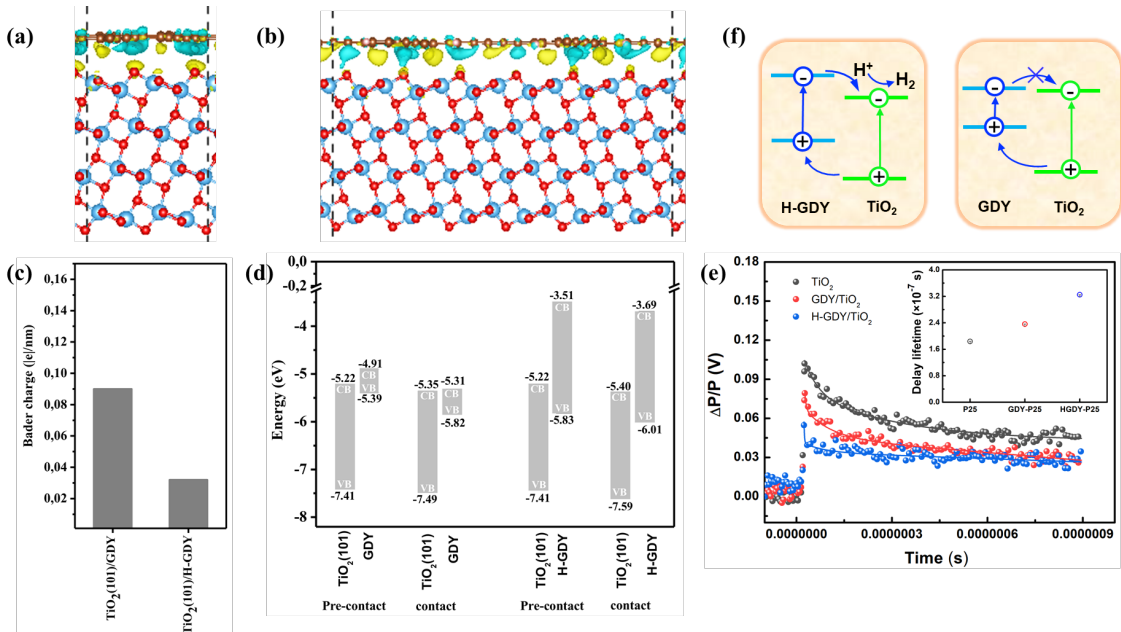
Figure 5: Side views of the 3D charge density difference in the (a) $TiO_2(101)/GDY$ and (b) $TiO_2(101)/H$-GDY heterostructures; isosurface values for 3D charge density difference plots are 0.09 $e/Å^3$; the accumulation and depletion of electrons are represented in cyan and yellow, respectively; (c) calculated Bader charge accumulated on the GDY (H-GDY) monolayer in the heterostructure; (d) relative band alignment of VB and CB band edges before and after the formation of the heterostructure. (e) TRMC measurements of TiO2, GDY/TiO_2 and $H-GDY/TiO_2$ at 360 nm; inside graph: the fitting of the delay lifetime of the three samples; (f) schematic illustration of the interfacial charge transfer between TiO_2 and H-GDY/GDY.

The amount of interfacial charge transfer in the two different systems are next quantified by using a Bader charge analysis (Figure 5c). In both cases, there is a charge transfer in the ground state between the two components, with the positive charge systematically localized in the H-GDY or GDY monolayer while the negative charge is localized in the TiO_2 slab, acting thus as the acceptor layer. This trend is rationalized by the small energy difference between the VB edge of GDY/H-GDY with respect to the CB edge of TiO_2. Interestingly, although the size of unit cell is smaller when considering GDY, the hole accumulation in GDY in the ground state is larger than that in H-GDY, most probably due to the larger carbon areal density in GDY. The pronounced hole accumulation in GDY also explains the large downward shifts of the VB and CB edges when going from the individual components to the blend (Figure 5d). It is also of prime interest to analyse the alignment of the band edges, which are key parameters that govern the charge transfer processes at the interfaces. As shown in Figure 5d, there is a large valence band offset ΔE_{VB} in the GDY/TiO_2 heterostructure while the conduction band minimum (CBM) of GDY is lying very close to that TiO_2. Under UV-visible light excitation of TiO_2, charges can be generated following an efficient photoinduced hole transfer between the valence bands of the two components whereas electron transfer processes between the conduction bands are expected to be much less efficient due to the absence of a significant driving force. For H-GDY/TiO_2 interfaces, there is a large offset between both the CBM and VBM of the two layers, leading to a type-II band alignment; photogenerated charge carriers are thus expected to be observed, originating from both efficient photoinduced hole transfer processes between the

valence bands (from TiO_2 to H-GDY) upon photoexcitation of TiO_2 and efficient photoinduced electron transfer processes between the conduction bands (from H–GDY to TiO_2) upon excitation of H-GDY. In turn, these two available pathways are expected to make the hydrogen evolution reaction more efficient.

To further elucidate and confirm the interfacial charge transfer between TiO_2 and H-GDY (GDY), a Time Resolved Microwave Conductivity (TRMC) analysis was performed under laser-pulsed excitation at 360 nm, which enables exciton generation in both materials. Compared to the well-known photoluminescence time resolved measurements, TRMC enables evaluating the dynamics of charge carriers in TiO_2-based composites.[45-46] Upon laser excitation of the samples, the concentration of the photogenerated charge carriers increased during the pulse, and then a subsequent decay is observed due to the decrease in the amount of excess charges, either by recombination, trapping or surface reaction processes. It is worth noting that no TRMC signal was observed for pristine H-GDY (GDY), probably due to the low sensitivity of the change in the conductivity of the carbon-based material. As shown in Figure 5e, pure TiO_2 shows higher maximum value of the signal than those of GDY/TiO_2 and H-GDY/TiO_2, which is probably attributed to the shield effect. However, these effects, usually harmful for the photoactivity, can be compensated by the influence on the charge carriers' lifetime (decay), a liming factor in the photocatalytic reaction.

In contrast to pure TiO_2, GDY/TiO_2 and H-GDY/TiO_2 exhibited much slower global decay, leading to a higher number of charge carriers exploitable for photocatalytic reactions. Notably, a lifetime of charge carriers of ~0.33 μs was observed in H-GDY/TiO_2, much longer than that for GDY/TiO_2 (~0.24 μs), thus indicating that the heterojunction between H-GDY and TiO_2 is more efficient for the charge separation than that between GDY and TiO_2, in full consistency with the theoretical analysis and experimentally observed photocatalytic activity. All in all, the charge carriers' separation in the H-GDY/TiO_2 and GDY/TiO_2 photocatalysts can be rationalized: GDY acts solely as a hole transport layer, while the H-substitution enables to

13

markedly increase the bandgap and provide well-disposed CB and VB bands to construct an efficient type II heterojunction with TiO_2, fully promoting a spatial charge carrier separation (Figure 5f), which subsequently improves the photocatalytic activity towards H_2 generation.

3. Conclusions

In conclusion, the electronic bandgap of GDY was adjusted by H-substitution and the obtained H-GDY was hybridized with TiO_2 to form a type II heterojunction. The prepared H-GDY/TiO_2 displayed excellent photocatalytic activity with H_2 production rate of ~6200 $\mu mol\ h^{-1}\ g^{-1}$ under UV-visible illumination and ~670 $\mu mol\ h^{-1}\ g^{-1}$ under visible illumination, which were 1.35 times higher and 4 times higher than that of GDY/TiO_2 composite, respectively. DFT calculations revealed that the superior activity of H-GDY is attributed to the suitable band alignment between H-GDY and TiO_2, which promote photogenerated electron and hole separation via different pathways compared to GDY/TiO_2 heterojunction. TRMC evidenced the longest lifetime of charge carriers in H-GDY/TiO_2, further evidencing the successful fabrication of type II heterojunction. The concept of tuning the electronic bandgap of GDY to construct efficient heterojunctions enhancing interfacial carrier separation is certainly not confined to H-substitution and TiO_2 but should be extended to other element doping and semiconductors for photocatalytic applications. Related works are in progress in our laboratory.

Reference:

1. X. Yang, D. Wang, *ACS Appl. Energy Mater.* **2018**, *1*, 6657-6693.

2. C. Xu, P. Ravi Anusuyadevi, C. Aymonier, R. Luque, S. Marre, *Chem. Soc. Rev.* **2019**, *48*, 3868-3902.

3. C. Dai, B. Liu, *Energy Environ. Sci.* **2020,** *13*, 24-52.

4. H. Wang, L. Zhang, Z. Chen, J. Hu, S. Li, Z. Wang, J. Liu, X. Wang, *Chem. Soc. Rev.* **2014**, *43*, 5234-5244.

5. J. Li, P. Jiménez-Calvo, E. Paineau, M. N. Ghazzal, *Catalysts* **2020**, *10*, 89.

6. Li, W. Zhu, C. Li, T. Wang, J. Gong, *Chem. Soc. Rev.* **2019**, *48*, 1874-1907.

7. F. Ning, M. Shao, S. Xu, Y. Fu, R. Zhang, M. Wei, D. G. Evans, X. Duan, *Energy Environ. Sci.* **2016**, *9*, 2633-2643.

8. T. Umeyama, H. Imahori, *Energy Environ. Sci.* **2008**, *1*, 120.

9. S. Ye, C. Ding, R. Chen, F. Fan, P. Fu, H. Yin, X. Wang, Z. Wang, P. Du, C. Li, *J. Am. Chem. Soc.* **2018,** *140,* 3250–3256.

10. S. Bellani, L. Najafi, B. Martín-García, A. Ansaldo, A. E. Del Rio Castillo, M. Prato, I. Moreels, F. Bonaccorso, *J. Phys. Chem. C* **2017**, *121*, 21887-21903.

11. U. Sim, J. Moon, J. An, J. H. Kang, S. E. Jerng, J. Moon, S.-P. Cho, B. H. Hong, K. T. Nam, *Energy Environ. Sci.* **2015**, *8*, 1329-1338.

12. X. Gao, H. Liu, D. Wang, J. Zhang, *Chem. Soc. Rev.* **2019**, *48*, 908-936.

13. C. Huang, Y. Li, N. Wang, Y. Xue, Z. Zuo, H. Liu, Y. Li, *Chem. Rev.* **2018**, *118*, 7744-7803.

14. J. Li, X. Gao, L. Zhu, M. N. Ghazzal, J. Zhang, C.-H. Tung, L.-Z. Wu, *Energy Environ. Sci.* **2020,** *13,* 1326-1346.

15. H. Yu, Y. Xue, Y. Li, *Adv. Mater.* **2019**, *31*, e1803101;

16. J. Li, X. Gao, Z. Li, J.-H. Wang, L. Zhu, C. Yin, Y. Wang, X.-B. Li, Z. Liu, J. Zhang, C.-H. Tung, L.-Z. Wu, *Adv. Funct. Mater.* **2019**, *29*, 1808079.

17. J. Li, X. Gao, X. Jiang, X.-B. Li, Z. Liu, J. Zhang, C.-H. Tung, L.-Z. Wu, *ACS Catal* **2017**, *7*, 5209-5213.

18. R. Sakamoto, N. Fukui, H. Maeda, R. Matsuoka, R. Toyoda, H. Nishihara, *Adv. Mater.* **2019**, *31*, e1804211.

19. N. Wang, J. He, K. Wang, Y. Zhao, T. Jiu, C. Huang, Y. Li, *Adv. Mater.* **2019**, *31*, e1803202.

20. X. P. Yin, H. J. Wang, S. F. Tang, X. L. Lu, M. Shu, R. Si, T. B. Lu, *Angew. Chem. Int. Ed.* **2018**, *57*, 9382-9386.

21. N. Yang, Y. Liu, H. Wen, Z. Tang, H. Zhao, Y. Li, D. Wang, *ACS Nano* **2013**, *7*, 1504-1512.

22. S. Thangavel, K. Krishnamoorthy, V. Krishnaswamy, N. Raju, S. J. Kim, G. Venugopal, *J. Phys. Chem. C* **2015**, *119*, 22057-22065.

23. J.-X. Lv, Z.-M. Zhang, J. Wang, X.-L. Lu, W. Zhang, T.-B. Lu, *ACS Appl. Mater. Interfaces* **2019**, *11*, 2655-2661.

24. Q. Xu, B. Zhu, B. Cheng, J. Yu, M. Zhou, W. Ho, *Appl. Catal B: Environmental* **2019**, *255*, 117770.

25. R. Wang, M. Shi, F. Xu, Y. Qiu, P. Zhang, K. Shen, Q. Zhao, J. Yu, Y. Zhang, *Nat. Commun.* **2020**, *11*, 4465.

26. F. Xu, K. Meng, B. Zhu, H. Liu, J. Xu, J. Yu, *Adv. Funct. Mater.* **2019**, *29,* 1904256.

27. G. Luo, X. Qian, H. Liu, R. Qin, J. Zhou, L. Li, Z. Gao, E. Wang, W.-N. Mei, J. Lu, Y. Li, S. Nagase, *Phys. Rev. B* **2011**, *84*, 075439.

28. M. Long, L. Tang, D. Wang, Y. Li, Z. Shuai, *ACS Nano* **2011**, *5*, 2593-2600.

29. T. Su, Q. Shao, Z. Qin, Z. Guo, Z. Wu, *ACS Catal* **2018**, *8*, 2253-2276.

30. J. Wang, S. Lin, N. Tian, T. Ma, Y. Zhang, H. Huang, *Adv. Funct. Mater.* DOI: *10.1002/adfm.202008008*.

31. H. Wang, B. Zhang, F. Zhao, B. Zeng, *ACS Appl. Mater. Interfaces* **2018,** *10,* 35281-35288.

32. U. Sim, T.-Y. Yang, J. Moon, J. An, J. Hwang, J.-H. Seo, J. Lee, K. Y. Kim, J. Lee, S. Han, B. H. Hong, K. T. Nam, *Energy Environ. Sci.* **2013**, *6*, 3658.

33. S. Zhao, D.-W. Wang, R. Amal, L. Dai, *Adv. Mater.* **2019**, *31*, 1801526.

34. H. Jin, C. Guo, X. Liu, J. Liu, A. Vasileff, Y. Jiao, Y. Zheng, S.-Z. Qiao, *Chem. Rev.* **2018**, *118*, 6337-6408.

35. G. Li, Y. Li, H. Liu, Y. Guo, Y. Li, D. Zhu, *Chem. Commun.* **2010**, *46*, 3256-3258.

36. J. Zhou, X. Gao, R. Liu, Z. Xie, J. Yang, S. Zhang, G. Zhang, H. Liu, Y. Li, J. Zhang, Z. Liu, *J. Am. Chem. Soc.* **2015**, *137*, 7596-7599.

37. H. Shang, Z. Zuo, H. Zheng, K. Li, Z. Tu, Y. Yi, H. Liu, Y. Li, Y. Li, *Nano Energy* **2018**, *44*, 144-154.

38. Y. Zhao, J. Wan, H. Yao, L. Zhang, K. Lin, L. Wang, N. Yang, D. Liu, L. Song, J. Zhu, L. Gu, L. Liu, H. Zhao, Y. Li, D. Wang, *Nat. Chem.* **2018**, *10*, 924-931.

39. Y. Kong, J. Li, S. Zeng, C. Yin, L. Tong, J. Zhang, *Chem* **2020**, *6*, 1933-1951.

40. C. Xing, Y. Xue, B. Huang, H. Yu, L. Hui, Y. Fang, Y. Liu, Y. Zhao, Z. Li, Y. Li, *Angew. Chem. Int. Ed.* **2019**, *58*, 13897-13903.

41. S. Zhuo, Y. Shi, L. Liu, R. Li, L. Shi, D. H. Anjum, Y. Han, P. Wang, *Nat. Commun.* **2018**, *9*, 3132.

42. T. Zhang, Y. Hou, V. Dzhagan, Z. Liao, G. Chai, M. Loffler, D. Olianas, A. Milani, S. Xu, M. Tommasini, D. R. T. Zahn, Z. Zheng, E. Zschech, R. Jordan, X. Feng, *Nat. Commun.* **2018**, *9*, 1140.

43. H. Pan, H. Zhang, H. Wang, J. Li, Y. Sun, W. Lu, X. Wang, *Applied Surf. Sci* **2020**, *513*, 145694.

44. Q. Lv, W. Si, J. He, L. Sun, C. Zhang, N. Wang, Z. Yang, X. Li, X. Wang, W. Deng, Y. Long, C. Huang, Y. Li, *Nat. Commun.* **2018**, *9*, 3376.

45. G. D. Gesesse, T. Le Neel, Z. Cui, G. Bachelier, H. Remita, C. Colbeau-Justin, M. N. Ghazzal, *Nanoscale* **2018**, *10*, 20140-20146.

46. C. Wang, J. Li, E. Paineau, A. Laachachi, C. Colbeau-Justin, H. Remita, M. N. Ghazzal, *J. Mater. Chem A* **2020**, *8*, 10779-10786.

Table of Contents:

Title: Tuning the Electronic Bandgap of Graphdiyne by H-substitution to Promote Interfacial Charge Carrier Separation for Enhanced Photocatalytic Hydrogen Production

By *Jian Li,[1] Amine Slassi,[2] Xu Han,[3] David Cornil,[2] Minh-Huong Ha-Thi,[4] Thomas Pino,[4] Damien P. Debecker,[5] François Devred,[5] Christophe Colbeau-justin,[1] Jordi Arbiol,[3,6] Jérôme Cornil,[2] Mohamed Nawfal Ghazzal[1]* *

Keywords: graphdiyne, electronic bandgap, charge carrier, photocatalysis, density functional theory (DFT)